A New Approach in the Modeling of the Critical Heat Flux and Enhancement Techniques

Khellil Sefiane
The School of Chemical Engineering, The University of Edinburgh, Edinburgh, EH9 3JL U.K.

Understanding of the boiling crisis mechanism is still incomplete; starting from experimental observations of the dry spots during boiling crisis, a new approach to bridge this gap is proposed. The thermal instabilities occurring at the triple contact lines where evaporation is intense are focused on. The "dry-out" phenomenon is local; it depends on the local conditions at a very tiny evaporating meniscus adjacent to the heating surface. The enhancing role of EHD for CHF is studied through a stability analysis of the meniscus subjected to an electrical-field. The equations describing the evaporating system are modified to account for the effect of electrical forces. We have found that the electrical-field delays thermocapillary instability. Our analysis revealed that the onset of instability is very sensitive to the interface deformation.

Introduction

Boiling heat transfer is an efficient method to handle high heat fluxes in numerous technological applications, such as compact heat exchangers, X-ray medical devices, high-power lasers, and fusion reactors. Heat loads for fusion-reactor components may require cooling schemes that can dissipate heat fluxes greater than 1 MW/M^2. The dry-out caused by exceeding the critical heat flux (CHF) is of major importance for heat-transfer devices involving a phase change (in the nuclear industry it may lead to catastrophic reactor damage). In several applications it has a serious influence on the deterioration of heat-transfer processes. Since the heat fluxes required for these applications exceed the CHF attainable with common flow boiling systems, the ability to both predict and increase the magnitude of CHF is therefore of paramount importance. A debate has been taking place for several years among researchers working in boiling on the mechanism controlling the boiling crisis. Understanding these processes is crucial because of the extensive use of heat exchangers to accommodate large heat fluxes in industry over the last several decades. There has been an increasing interest in the investigation of the CHF mechanism and numerous studies have been devoted to this problem. Since then, scholars have emerged on the leading mechanism of CHF, in particular the hydrodynamic instability theory, Zuber (1958) and the microlayer theory, and Haramura and Katto (1982), have gained wide acceptance in the scientific community. However, the challenge for a unified mechanistic theory remains unsolved. Several models have been proposed, but none of them brings a convincing response to the unanswered challenging problems, such as boiling behavior under reduced pressure, or boiling in microgravity where the previous theories are no longer applicable, as shown by Straub (1991) and Ervin et al. (1992). In particular, hydrodynamic theories have been demonstrated to be invalid under many conditions (cf. microgravity, small heaters, low pressure) (Katto, 1994). These results question the assumption that the critical heat flux is controlled by a hydrodynamic instability. Indeed, an understanding of the major controlling mechanism during the CHF occurrence is still incomplete. Several recent reviews have pointed out this issue (Sadasivan et al., 1994), and the issue of explosive boiling has been reported in previous works. Many researchers have pointed out the role played by the triple-line region and the contact line between liquid, vapor, and solid that is not accounted for in the hydrodynamic and microlayer theory (Wayner, 1994). It is well known from experimental observations that on approaching the critical heat flux, dry spots form on the heating surface, which later, nearer the CHF, start to oscillate. The dry-out phenomenon occurs when dry spots spread over the heating surface, leading to a transition to film boiling. In this work it is suggested that the controlling mechanism for boiling crisis is due to the instabilities occurring at the triple line of the evaporating meniscus, leading to the wearing-off and dry-out. Instabilities responsible for such a mechanism originate from the high evaporation rates and thermal constraints present at the edge of the evaporating meniscus. An explosive type of vapor bubble

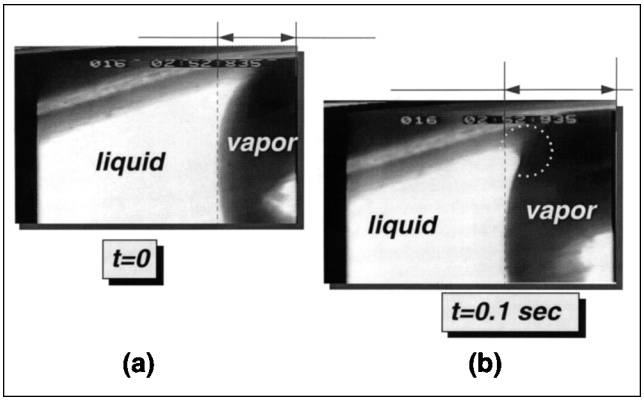

Figure 1. Observed of pentane meniscus in a 1-mm capillary pore receding (from the experiments of Pratt et al., 1998).

(a) Just prior to the origination of instability, and (b) 1/10 s later.

growth was observed in recent experiments on boiling in microgravity (Lee and Merte, 1998). These researchers considered the instability of the interface in order to explain the vapor explosion behavior. According to their observations, the vapor seems to spread over the heating solid. These observations, as well as recent experimental work on the evaporation of menisci in capillaries (Pratt et al., 1998), suggest the existence of a new mechanism based on instabilities occurring in the evaporating menisci. Observations reported by Pratt et al. (1998) (Figure 1), revealed the instability mechanism to be operating at very small length and time scales (tenths of second). The experiments were performed on evaporating menisci in heated tubes of 0.5 to 3 mm in diameter, which makes the analogy with evaporating menisci in boiling stems well justified. The observations of Pratt et al. demonstrated the onset of instabilities at the edge of an evaporating meniscus where the wetting contact angle increases suddenly. The receding meniscus follows the increase in the contact angle. These observations suggest an analogy with the mechanism of boiling crisis, that is, the dry-out phenomenon occurs starting from the triple line, which is subjected to high thermal stresses. Pratt et al. referred to the thermocapillary instability to explain their observations. This instability causes the evaporating meniscus to recede, leading to the observed dry-out, as described in the observations of Pratt et al. (1998). The instability is triggered near the contact line, and thus reinforces the proposed mechanism for CHF in the model introduced in this article, that is, these recent revelations confirm our former theory (Sefiane et al., 1998), about the likelihood of the controlling mechanism leading to dry-out. This theory, when further verified, can replace the existing models of the CHF mechanism, which proved to be unsatisfactory for many conditions.

The recoil instability as observed by Hickman (1952) and later analyzed by Prosperetti and Plesset (1984) is found to occur over hundredths of a second. The fact that both the thermocapillary and the recoil instabilities operate at a very short time scale makes the observations very difficult in the case of boiling heat transfer.

Electrohydrodynamic Effect at the Critical Heat Flux

The need to conserve energy has led to an increased effort by the scientific community to improve the efficiency of heat-transfer enhancement in both single- and two-phase heat-transfer processes. Enhancement techniques are categorized as passive or active. The former does not require use of external power, whereas the latter require some direct use of power for the enhancement. The passive category includes treated, rough, and extended surfaces, displacement enhancement devices, swirl flow devices, and so forth. Surface and fluid vibration, suction or injection, mechanical aids, and high-intensity electrostatic fields are examples of active enhancement technique (Bergles, 1997). The increase of the heat-transfer coefficients in heat exchangers can be achieved by either (1) a reduction in the heat exchange areas, (2) a reduction in the temperature difference between fluids exchanging heat, or (3) an increase in the thermal capacity for a given size and temperature difference. Enhancement of the thermal capacity can be critical in a plant where an increased load may be required beyond that envisaged at the design stage due to some unforeseen demand. Reay (1991) provided a detailed analysis of the possibilities of various enhancement techniques, indicating also that enhancement can lead to environmental improvements.

The possibility of using an intense electric field to enhance heat transfer rates, termed electrohydrodynamic (EHD) heat transfer, had been reported as early as 1916 (Chubb, 1916). The application of EHD requires an electrode to be placed near the active heat-transfer surface. In most cases, high voltage is applied at the electrode while the surface is earthed. The particular advantages of using EHD in heat-transfer enhancement may include:

1. Simple control of the heat-transfer coefficient by controlling the voltage
2. Simple implementation—integration
3. No moving parts—reliability
4. External power consumed is in most cases negligible (usually a few watts)
5. Negligible pressure loss increase.

In addition, EHD can eliminate boiling hysteresis and contribute to the eradication of "start-up" problems in plants operating with small temperature differences, where the degree of superheat required for ebullition may not be available at the beginning of the process. Further, EHD can be beneficial in the presence of oil in the working fluid by countering the reduction of heat transfer that it may cause. The negligible current of EHD applications makes this technique safe to use. Allen and Karayiannis (1995) suggested that EHD enhancement of boiling (and condensation) can be attributed to the following factors, which can act individually or in combination: (a) action at liquid–vapor interface, (b) action on vapor bubbles; and (c) change in surface tension and contact angle. EHD has been reported to augment boiling heat-transfer rates in the lower nucleate regime, but the highest improvements have been reported at the peak (and minimum film) boiling conditions. In effect EHD "extends" the nucleate boiling regime to higher q and ΔT. However, the complexity and uncertainty in the mechanism that determines the occurrence of the CHF limited the analytical efforts of the

researchers and most of the reported past work is experimental (Allen and Karayiannis, 1995). Zhorzholiani and Shekriladze (1972) reported that the CHF of boiling acetone increased by a factor of 2.14 when the electric field applied was 0.9 MV/m. Similar increases were reported by Choi (1962) for R113. Markels and Durfee (1964, 1965) studied EHD boiling in semi-insulating liquids such as isopropyl alcohol and deionized water. The CHF was increased by up to five times by application of 8 kV dc. Bologa et al. (1988) studied EHD boiling heat transfer in slot channels with R113, pentane, and diethyl alcohol, and found an increase of up to three times. Winer (1967) used R114 boiling on a cylindrical heater and a radial electric field and reported an increase of more than 40% in the CHF at 5 kV/m. An improvement up to six times for R113 at 40 kV was also reported by Asch (1966).

In a recent review chapter, Yabe et al. (1996) suggested using electric-field effects to analyze the dynamic mechanism of the CHF. One such attempt with an applied electric field < 2 MV/m is described by Takahashi et al. (1994). They used a high-speed camera and a capacitance probe to measure the variation of the thickness of a thin liquid film on a heat-transfer surface at the bottom of a boiling bubble and the length of tiny circular vapor stems on the surface at CHF. They reported that, under the influence of the field, nearly continuous vapor columns grow in the direction of the field and that the bubbles were not broken up near the heat-transfer surface or near the top of the circular vapor stems. The average time period for the departure of one set of bubbles was smaller with the electric field applied (from 45–55 ms to less than 30 ms), and this shorter period was related to the augmentation of the CHF. The researchers concluded that analyzing the mechanism causing this shorter time period was important in analyzing the mechanism causing the CHF. Hydrodynamic theory has been extended previously to the analysis of CHF with an electric field. Berghmans (1978) considered a flat heater located in a conducting liquid and performed a stability analysis including the effect of a uniform dc field. He developed a surface-wave theory to predict the effect of the electric-field on the CHF. In his analysis for a conducting liquid, he included the electric-field induced force at the liquid–vapor interface to obtain an expression for the

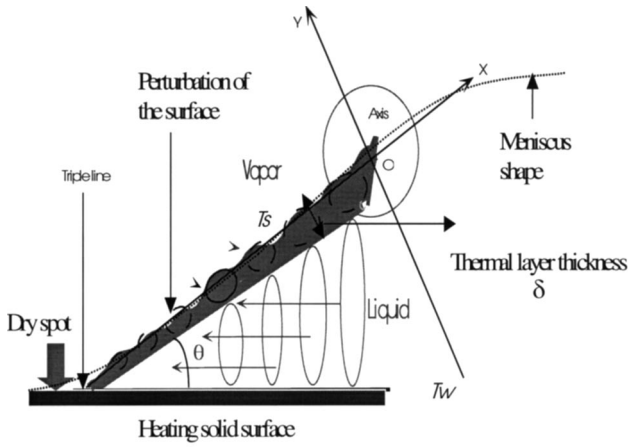

Figure 2. Model for the triple line and evaporating meniscus.

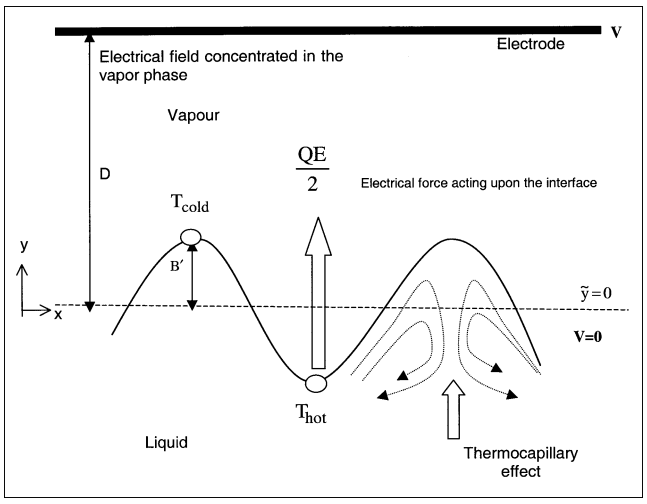

Figure 3. Perturbed interface and various effects.

wavelength of the perturbation with the largest growth rate. This analysis resulted in an equation for the CHF, including the applied electric-field strength that was compared with the small number of data points of Markels and Durfee (1964). The choice of the vapor film thickness was considered to be a possible reason for the deviations of the theory from the experiments. Johnson (1968) amended the hydrodynamic theory to include the effect of a perpendicular electric field across the liquid–vapor interface that exists at the maximum (and minimum heat flux) and correlated the ratio $q_{c,E}/q_{c,o}$ as a function of fluid properties and electric-field strength. He assumed that the only EHD coupling mechanism was at the liquid-vapor interface. The resulting equation for the maximum heat-flux condition was compared with the experimental results of Winer (1967). The experimental results were limited, however, and no firm conclusions could be drawn. Di Marco and Grassi (1995) carried out an energetic theoretical analysis and concluded that the effect of the electric field on the interface stability can be fully described by means of 2-D groups, E^* and k (electrical number and wavelength).

The coupling mechanism of EHD at the liquid–vapor interface was also used more recently by Verplaetsen and Berghmans (1996) to study the electric field effect on film boiling for a conducting fluid. The additional interfacial force (Maxwell stress, normal to the interface and directed from the liquid to the vapor (see Figure 3)), was included in the analysis that concluded that EHD affects both the distance between vapor bubbles at the interface and their shape. Their analysis demonstrated a possible increase in the heat-transfer coefficient of up to 10 times when the electric influence number is about 5.

In the present work we propose to study the enhancement effect due to the electric field through the stability of the evaporating meniscus adjacent to the heating surface. This could be used in confirming the new approach to the modeling of CHF and enhancement techniques.

Mathematical Formulation

An evaporating meniscus is described in Figure 1. The coordinate system chosen is such that the "x" coordinate is on

the evaporating interface and the "y" coordinate to be normal to it. At the interface a thermal boundary layer of thickness δ is supposed to exist, where heat transfer is purely conductive (Figure 2). The approach used is to write equations describing the evaporating meniscus, with additional terms taking into account the effect of the electrical field (equations in bulk liquid, bulk vapor, and at the interface). The velocity of the interface v^i is dictated by the evaporation rate, and has two components in this model (v_x^i, v_y^i). Taking a linear profile for the evaporation rate will give velocity ω, components described by an angular velocity which gives the two components as $v_x^i = \omega x$ and $v_y^i = \omega y$. Since the dielectric permeability of the liquid is much higher than vapor, then the electrical field is mainly concentrated in the vapor phase.

General Form

For incompressible fluids the conservation equations for mass, momentum, and energy are

$$\nabla \cdot u = 0 \tag{1}$$

$$\rho \frac{\partial u}{\partial t} + \rho(u \cdot \nabla)u = -\nabla P + \rho \upsilon \nabla^2 u \tag{2}$$

$$\frac{\partial T}{\partial t} + u \cdot \nabla T = \kappa_L \nabla^2 T. \tag{3}$$

In the preceding equations, P is the pressure tensor including Maxwell tensor. Taking into account the presence of the electrical force, the boundary conditions at the liquid–vapor interface are expressed. The following equations are written: mass, continuity of the tangential component of velocity, energy conservation, normal, and tangential components of momentum.

Perturbed System

By adopting a linear stability analysis, the basic equations representing the steady state of the system are the conservation of mass, momentum, and energy at the interface. The system of equations is now perturbed by an infinitesimal amount (primed quantities) from their quiescent values (starred quantities). We introduce in our system a perturbation in the form of a surface wave with a wave number, k. The interface at the steady state ($y = 0$) is then displaced by an amount B' in the y-direction, where $B' = \langle B \rangle e^{i\omega t} e^{i(kx)}$, $\langle B \rangle$ is the amplitude of the perturbation. This perturbation of the interface will give rise to corresponding perturbations in the pressure, velocity, and temperature fields:

$$p' = \langle P \rangle e^{i\omega t} e^{ikx}, \qquad W' = \langle W \rangle e^{i\omega t} e^{ikx}, \qquad T' = \langle T \rangle e^{i\omega t} e^{ikx}.$$

We apply twice the curl operator ($\nabla \wedge$) to the momentum equation to eliminate the pressure terms, and we neglect the gravity term in the bulk equations as well as second-order terms. We make the assumption of exchange of stability (the real and imaginary parts of the time growth constant are set equal to zero). We then get for a single normal mode of the perturbation, after making some mathematical rearrangement (Sefiane, 1998), that:

Momentum equation leads to the following expression:

$$\nabla^2 \left[\nu \nabla^2 W' - \omega y \frac{\partial}{\partial x} W' + \omega x \frac{\partial}{\partial y} W' \right] = 0, \tag{4}$$

where W' is the perturbation in the normal component of the velocity field.

For a single normal mode of the perturbation, we get

$$(D^2 - k^2)\left[\nu (D^2 - k^2) + \omega x D - ik\omega y \right] W' = 0 \tag{5}$$

with $D = \partial/\partial y$.

The energy equation (Eq. 3) is written as

$$\left[\kappa_L (D^2 - k^2) - (ik\omega y - \omega x D) \right] T_L' = \begin{cases} -\beta W_L' & -\delta < y < 0 \\ 0 & -\infty < y < -\delta. \end{cases} \tag{6}$$

The general conservation equations at the liquid–vapor interface are given below: The mass balance across the interface is given by

$$J = \rho_\upsilon (V_\upsilon - V^i) \cdot n = \rho_L (V_L - V^i) \cdot n, \tag{7}$$

where $V^i = dB'/dt$ is the interfacial velocity. The continuity of the tangential component of velocity is given by

$$(V_\upsilon - V_L) \cdot t = 0. \tag{8}$$

The energy balance across the interface expressed by

$$J\left\{ H_{fg} + \frac{1}{2}\left[(V_\upsilon - V^i) \cdot n \right]^2 - \frac{1}{2}\left[(V_L - V^i) \cdot n \right]^2 \right\} - k_\upsilon \nabla T_\upsilon \cdot n + k_L \nabla T_L \cdot n + (V_\upsilon - V^i).\left[2\mu_L (\hat{T}_L \cdot n) - 2\mu_\upsilon (\hat{T}_\upsilon \cdot n) \right] = 0. \tag{9}$$

The normal momentum balance is represented by

$$J(V_L - V_\upsilon) \cdot n - \left(\hat{T}_L - \hat{T}_\upsilon \right) \cdot n \cdot n = \sigma \nabla \cdot n + \epsilon_L (E_L \cdot n)^2 - \epsilon_\upsilon (E \cdot n)^2 - \frac{\epsilon_L}{2} E_L \cdot E_L + \frac{\epsilon_\upsilon}{2} E \cdot E. \tag{10}$$

The tangential momentum balance is given by

$$\left(\hat{T}_\upsilon - \hat{T}_L \right) \cdot n \cdot t = \epsilon_L (E_L \cdot n)(E_L \cdot t) - \epsilon_\upsilon (E \cdot n)(E \cdot t). \tag{11}$$

Using the preceding general form of conservation equations at the interface and neglecting the second-order terms as well as negligible terms in vapor and liquid, and neglecting heat conductivity of vapor before the one in liquid, the following boundary conditions are given. The mass and continuity of

the tangential velocity balance read:

$$\rho_L W_L - \rho_v W_v' = \frac{dB'}{dt}(\rho_L - \rho_v), \tag{12}$$

or

$$J' = \rho_L W_L' - \rho_L \frac{dB'}{dt} = \rho_v W_v' - \rho_v \frac{dB'}{dt} = \rho_L v_i'. \tag{13}$$

Continuity of tangential velocity gives:

$$J^*\left(1 - \frac{\rho_L}{\rho_v}\right)\nabla^2 B' = \frac{\partial W_L'}{\partial y} - \frac{\partial W_v'}{\partial y}. \tag{14}$$

The normal component of the interfacial momentum balance reads:

$$(P_L' - P_v') = 2J^*J'\left(\rho_V^{-1} - \rho_L^{-1}\right) + 2\left(\mu_L \frac{\partial W_L'}{\partial y} - \mu_v \frac{\partial W_v'}{\partial y}\right) - \sigma^* \frac{\partial^2 B'}{\partial x^2} + \frac{QE}{2} = 0. \tag{15}$$

We can see in the preceding equation, describing the conservation of the normal momentum, that an extra term related to the electrical effect through density of the electric force is present Berghmans, (1978). The same equation is written at $y = 0$ using a Taylor series. It is then written in such a way as to provide an analysis of the effect at the electrical forces. The electrical field, combined with the charge density, will give the force density, which acts on the liquid–vapour interface $QE/2$.

Writing Eq. 15 is equivalent to taking into account the effect of the electrical field on the surface tension term through $\sigma = \sigma^* - (QE/2)$. The electrical force is directed from the liquid to the vapor. This relationship can be used to analyze the effect of the electrical field and to propose the mechanism that operates. Equation 15 describes the normal pressure pattern of the surface. In the absence of mass flux, P_L' is positive under the crests and negative under the troughs; this pressure distribution tends to damp the perturbation. (As to the effect of the electric force, which is directed into the vapor phase in the crests, the pressure in the liquid counters it, whereas in the troughs it acts to damp down the perturbation.) In the presence of the thermocapillary effect, liquid driven from the troughs to the crests amplifies the perturbation. In troughs, the electrical force tends to damp the perturbations and act against the thermocapillary effect (Figure 3). The electric field is related to the charge density Q by the following relationship:

$$Q = \epsilon_v E.$$

After the development of the electrical-field perturbation in the preceding expression, we get:

$$(P_v' - P_L') + 2J^*J'\left(\rho_v^{-1} - \rho_L^{-1}\right) + 2\left(\mu_L \frac{\partial W_L'}{\partial y} - \mu_v \frac{\partial W_v'}{\partial y}\right) - \sigma^* \frac{\partial^2 B'}{\partial x^2} + g(\rho_L - \rho_v)B' + \epsilon_g E^0 E_y' = 0. \tag{16}$$

Because the perturbed electric field can be derived from a potential E_y', a solution could be developed in the form [see Berghmans (1978)]:

$$E_y' = B' E^0 k \coth kD \quad \text{at} \quad y = 0,$$

where D is the distance between the liquid–vapor interface and the electrode. The normal momentum balance is written as follows:

$$(P_v' - P_L') + 2J^*J'\left(\rho_V^{-1} - \rho_L^{-1}\right) + 2\left(\mu_L \frac{\partial W_L'}{\partial y} - \mu_V \frac{\partial W_v'}{\partial y}\right) - \sigma^* \frac{\partial^2 B'}{\partial x^2} + g(\rho_L - \rho_v)B' + \epsilon_g E^{0^2} B' k \coth kD = 0. \tag{17}$$

The tangential component of the interfacial momentum balance reads:

$$\mu_L\left(\nabla_n^2 W_L' - \frac{\partial^2 W_L'}{\partial y^2}\right) - \mu_v\left(\nabla_n^2 W_v' - \frac{\partial^2 W_v'}{\partial y^2}\right) = \nabla_n^2 \sigma'. \tag{18}$$

At the reference surface, $y = 0$, we have to account for the variation of surface tension with temperature expanding T' in a Taylor series about $y = 0$:

$$\nabla_n^2 \sigma' = \left(\frac{\partial \sigma}{\partial T}\right)\nabla_n^2 T_L'|_{y = B'}$$

$$T_L'|_{y = B'} = T_L'|_{y = 0} - \beta B'.$$

The conservation of energy at the interface (neglecting the kinetic term, which is usually much smaller than the latent heat term) is given as:

$$H_{fg} J' + k_L \frac{\partial T_L'}{\partial y} - 2J^*\left(\frac{\mu_V}{\rho_V}\frac{\partial W_v'}{\partial y} - \frac{\mu_L}{\rho_L}\frac{\partial W_L'}{\partial y}\right) = 0. \tag{19}$$

Scaling

The perturbations, as well as the expected instability, occur at the thermal boundary-layer scale. The scaling factors are chosen to be related to the transfer properties in the thermal layer, and length is scaled on the thermal-layer thickness, which depends on the position, x. According to the model proposed in Figure 2, $\delta = (X_i - x)\delta\alpha$. Velocity in the vapor is scaled by the ratio of the characteristic times of heat diffusion to viscous dissipation, which introduces the momentum

transfer at the interface, $(\kappa_L \mu_L/\mu_v \delta)$. The hydrodynamic velocity in the liquid is scaled by the thermal diffusivity through the layer κ_L/δ. Pressure in liquid and in vapor is usually scaled by $(\mu_L \kappa_L)/\delta^2$. Temperature is scaled by the temperature difference through the layer $\beta\delta$.

Momentum balance in the liquid, the vapor, and the energy balance are given in the dimensionless form:

$$(\tilde{D}^2 - \tilde{k}^2)\left[\tilde{D}^2 - \tilde{k}^2 - R_e\left(\tilde{D} - \frac{\tilde{y}}{\tilde{x}} i\tilde{k}\right)\right]\tilde{W}_L = 0 \quad (20)$$

$$(\tilde{D}^2 - \tilde{k}^2)\left[\tilde{D}^2 - \tilde{k}^2 - R_e N_\mu\left(\tilde{D} - \frac{\tilde{y}}{\tilde{x}} i\tilde{k}\right)\right]\tilde{W}_v = 0 \quad (21)$$

$$\left[\tilde{D}^2 - \tilde{k}^2 - R_e P_r\left(\tilde{D} - \frac{\tilde{y}}{\tilde{x}} i\tilde{k}\right)\right]\tilde{T}_L = \begin{cases} -\tilde{W}_L & -1 < \tilde{y} < 0 \\ 0 & -\infty < \tilde{y} < -1. \end{cases} \quad (22)$$

Equations 20, 21, and 22 can be solved for $\tilde{y}/\tilde{x} \approx \xi$, where ξ is a small parameter of first order. This condition is fulfilled at the edge of the triple line (Figure 2) where evaporation is greatest. This region is potentially the most unstable, because the high evaporation rate its instability causes will trigger the destabilization of the whole thermal layer. Equations 20, 21, and 22 then reduce to:

$$(\tilde{D}^2 - \tilde{k}^2)\left(\tilde{D}^2 - \tilde{k}^2 - R_e\tilde{D}\right)\tilde{W}_L = 0 \quad (23)$$

$$(\tilde{D}^2 - \tilde{k}^2)\left(\tilde{D}^2 - \tilde{k}^2 - R_e N_\mu \tilde{D}\right)\tilde{W}_v = 0 \quad (24)$$

$$\left(\tilde{D}^2 - \tilde{k}^2 - R_e P_r \tilde{D}\right)\tilde{T}_L = \begin{cases} -\tilde{W}_L & -1 < \tilde{y} < 0 \\ 0 & -\infty < \tilde{y} < -1 \end{cases}. \quad (25)$$

After scaling Eq. 12, Eqs. 14 and 17–19 become, respectively:

$$R_e P_r C_r\left(1 - N_p^{-1}\right)\tilde{W}_v - H_i\left[\tilde{T}_L - \tilde{B}\right] = 0 \quad (26)$$

$$N_p\tilde{W}_L - N_\mu\tilde{W}_v = 0 \quad (27)$$

$$N_\mu D\tilde{W}_v - D\tilde{W}_L + R_e P_r(N_P - 1)\tilde{k}^2\tilde{B} = 0 \quad (28)$$

$$C_r\left(\tilde{P}_L - \tilde{P}_v\right) + 2C_r\left(D\tilde{W}_v - D\tilde{W}_L\right) - 2H_i\left(\frac{N_\mu}{P_r}\right)\left(\tilde{T}_L - \tilde{B}\right) - \left(\tilde{k}^2 + B_o\right)\tilde{B} + E^*\tilde{k}\tilde{B}\coth(\tilde{k}D) = 0 \quad (29)$$

$$\tilde{k}^2 M_a\left(\tilde{T}_L - \tilde{B}\right) + D^2\tilde{W}_L - D^2\tilde{W}_v + \tilde{k}^2\left(\tilde{W}_L - \tilde{W}_v\right) = 0 \quad (30)$$

$$P_r D\tilde{T}_L + 2B_r\left(D\tilde{W}_L - N_p D\tilde{W}_v\right) = 0. \quad (31)$$

At the bottom of the thermal boundary layer the liquid temperature at

$$\tilde{y} = -1, \tilde{T}_L, \quad \text{and} \quad \partial\tilde{T}_L/\partial\tilde{y} \quad (32)$$

must be continuous.

Solutions

Solving the bulk equations (Eqs. 23, 24 and 25) leads to:

$$\tilde{W}_v = C_{11}e^{-\tilde{k}\tilde{y}} + C_{12}e^{1/2[R_e N_\mu - (R_e^2 N_\mu^2 + 4\tilde{k}^2)^{1/2}]\tilde{y}} \quad (33)$$

$$\tilde{W}_L = C_{21}e^{\tilde{k}\tilde{y}} + C_{22}e^{1/2[R_e - (R_e^2 + 4\tilde{k}^2)^{1/2}]\tilde{y}} \quad (34)$$

$$\tilde{T}_L = C_{31}e^{\frac{1}{2}\left[-R_e P_r + \left(R_e^2 P_r^2 + 4\tilde{k}^2\right)^{1/2}\right]\tilde{y}} + C_{32}e^{\left(R_e Pr + \frac{1}{2}\left[R_e P_r - \left(R_e^2 P_r^2 + 4\tilde{k}^2\right)^{1/2}\right]\right)\tilde{y}} + \frac{C_{21}}{\tilde{k}R_e Pr}e^{\tilde{k}\tilde{y}} + C_{22}\Big/\frac{1}{2}\left[-R_e + \left(R_e^2 + 4\tilde{k}^2\right)^{1/2}\right] \times R_e(Pr - 1)e^{1/2[-R_e + (R_e^2 + 4\tilde{k}^2)^{1/2}]\tilde{y}} \quad -1 < \tilde{y} < 0 \quad (35)$$

$$\tilde{T}_L = C_{33}\frac{1}{2}\left[-R_e P_r + \left(R_e^2 P_r^2 + 4\tilde{k}^2\right)^{1/2}\right]\tilde{y} \quad -\infty < \tilde{y} < -1, \quad (36)$$

Where c_{11}, c_{12}, c_{21}, c_{22}, c_{31}, c_{32}, c_{33} are integration constants.

Equations 33, 34, and 35 are substituted in the boundary (Eqs. 26–32). Evaluating at $\tilde{y} = 0$ and eliminating pressure by use of momentum conservation in the bulk, we obtain then a system of equations of the form:

$$A \cdot C = 0 \quad (37)$$

where (A) is a matrix relating all the parameters (M_a, R_e, H_i, C_r, B_o, P_r, N_μ, N_ρ, ...) to the wave number k, and C is the matrix describing the integration constants

$$\mathrm{Det}(A) = 0. \quad (38)$$

This condition will give the dispersion relation. The marginal stability curve is obtained from the dispersion relation (Eq. 38) by plotting the Marangoni number against the wave number. Figure 4 gives the curve separating stable regions from unstable ones. The minimum point on this curve represents

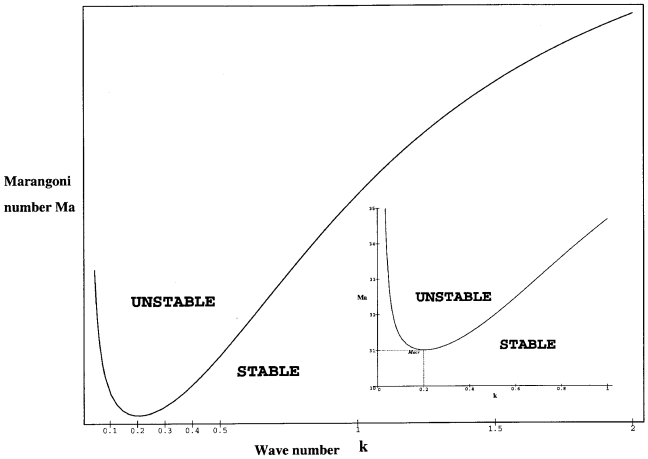

Figure 4. Marginal stability curve from (Eq. 33).

$H_i = 0$, $C_r = 10^{-3}$, $B_o = 1$, $N_\mu = 300$, $B_r = 0$, $P_r = 30$, $N_\rho = 10^5$, $R_e = 0.01$, $E^* = 0$.

the least constraint, corresponding to the Marangoni number from which unstable states are triggered. The Marangoni number value corresponding to this minimum is designated as the "critical Marangoni number"; it will be used as the main parameter indicating the threshold for the onset of thermocapillary driven instability.

We can see that the minimum of the marginal stability curve occurs at a finite wave number of 0.2. In the following sections calculations are performed to investigate how the threshold of the instability is influenced by the application of an electrical field.

Discussion

The boiling crisis is the overheating of a surface starting from the formation of a hot, dry patch underneath a bubble or a vapor column. The behavior of these dry patches and the local heat flux is thought to determine the CHF. Little is known, however, of the mechanism controlling the start of the boiling crisis. In subcooled boiling, the onset of CHF corresponds to the drying out of a liquid film under one of the larger vapor bubbles, or "mushrooms." It has been suggested that the appropriate mechanism in the subcooled region is the spreading of a dry patch following microlayer evaporation under a bubble, while in saturated boiling the mechanism is thought to be that of dry-out. Several alternative mechanisms for the dry-out of the liquid film on a heated surface have been proposed:

- Simple dry-out due to the inability of the deposition of droplets to make up for the loss of liquid by evaporation
- Rivulet patterning of liquid film followed by breakup of the liquid film below a certain critical liquid flow rate, causing a local dry-out
- Strong liquid reentrainment in the vapor core to dry out the liquid film
- Breakup of the liquid film due to the growth of bubbles at nucleation sites—comparable to pool boiling.

The mechanism we introduce in this article is based on the role of interfacial instabilities (thermocapillary, recoil, or inertial) in triggering the mechanism for dry-patch enlargement. The approach adopted is a stability analysis of the evaporating meniscus adjacent to the dry patches. In this study we limited the analysis to thermocapillary instability, which is likely to prevail in many situations.

Concerning EHD enhancement of CHF, Collier (1972) described the improvement of CHF through the use of electric fields. The application of an electric field to pool boiling results in large increases in the CHF. Yabe (1996) increased the CHF in R113 by 20% using uniform electric-field strength of 20 kV/cm. Many other researchers have reported and confirmed the enhancement of CHF when applying an electric field.

As discussed earlier, several theories have been proposed for boiling crisis, only one of which, the hydrodynamic theory, has been applied to the electrohydrodynamic situation. The theoretical results of Johnson and Berghams are, however, not supported by sufficient experimental evidence. We think that more research is needed, both in this field and to investigate the effect of EHD in the other approaches to the critical heat flux.

In this article, the stability of the evaporating meniscus as well as the influence of the electrical field will be investigated in terms of the influence of the voltage, distance to the electrodes, and electrical number on the instability threshold, given by the critical Marangoni number, Ma_{cr}. The variation in Ma_{cr} as a function of the electrical number E^*, is shown in Figure 5. The threshold of unstable states is increased and the stable region is enlarged at higher values of Ma_{cr}.

The following conclusion could be proposed to account for the data shown in Figure 5: increasing the value of the electrical number, E^*, will increase the threshold of the unstable regions, implying that the onset of instability is delayed by increasing the electrical number. The electrical number includes the electrical-field intensity, revealing the role of electrical-field application in the delay of the onset of the instability mechanism.

The influence of the crispation number reflects the effect of the interface deformation, which is illustrated in Figure 6. The crispation number is the ratio of the viscous dissipation

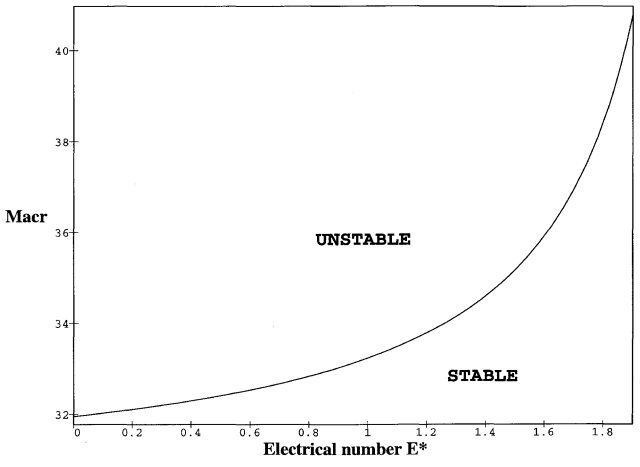

Figure 5. Critical Marangoni number vs. E *.

$H_i = 0,\ C_r = 10^{-3},\ B_o = 1,\ B_r = 0,\ N_\mu = 300,\ P_r = 30,\ N_\rho = 10^5,\ R_e = 0.01.$

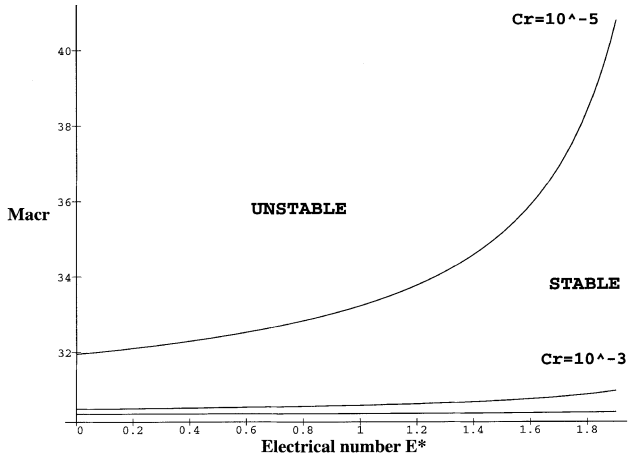

Figure 6. Critical Marangoni number vs. electrical number for various crispation number.

$H_i = 0,\ B_o = 1,\ N_\mu = 300,\ P_r = 30,\ B_r = 0,\ N_\rho = 10^5,\ R_e = 0.01.$

to surface tension over length scales of the order of δ. Vanishing values of the crispation number may correspond to infinite surface tension and an undeformable interface. In the opposite case the capillary number diverges to infinity when one approaches a critical point or for very thin liquid samples. In practice, its value can be related to the surface deformation in a liquid layer. Typically the crispation number in standard thermocapillary convection is small, typically 10^{-3}–10^{-7}. Figure 6 indicates that a decreasing crispation number leads to a more stable system. The threshold of the themocapillary instability is delayed as the crispation number decreases, demonstrating that the more deformable interfaces are subject to greater instability.

In Figure 7 it is shown that increasing the density ratio delays the instability. The density ratio could be related to the operating pressure, reducing pressure results in larger density ratios. Under these conditions other kinds of instabilities, such as the vapor recoil effect, may prevail.

In order to have a more detailed idea about the influence of the electrical field, resulting from the application of a voltage through a distance D, the influence of both these parameters is investigated (Figure 8). The increase in the voltage is found to stabilize the interface, whereas the distance to the electrode (D) is found to decrease the threshold when it is increased. This confirms that the stabilizing effect is due to the influence of the electrical field.

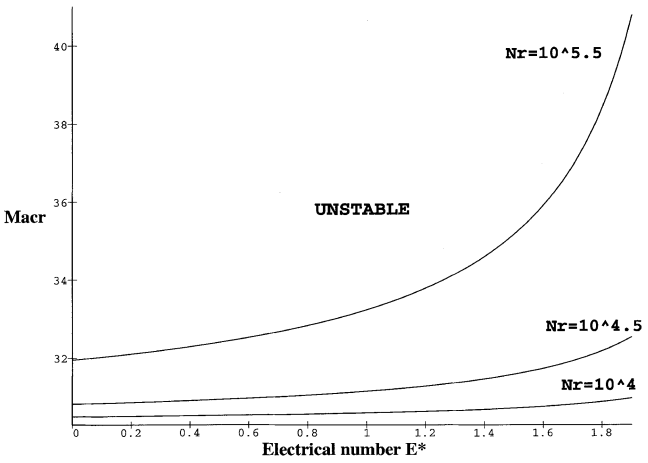

Figure 7. Critical Marangoni number vs. electrical number for different density ratios.

$H_i = 0$, $C_r = 10^{-3}$, $B_o = 1$, $N_\mu = 300$, $B_r = 0$, $P_r = 30$, $N_\rho = 10^5$, $R_e = 0.01$.

In the following section, the influence of the Bond number is investigated. The Bond number is the ratio of surface tension effects to the effect of gravity over a length scale δ. The evolution of the threshold for the thermocapillary instability

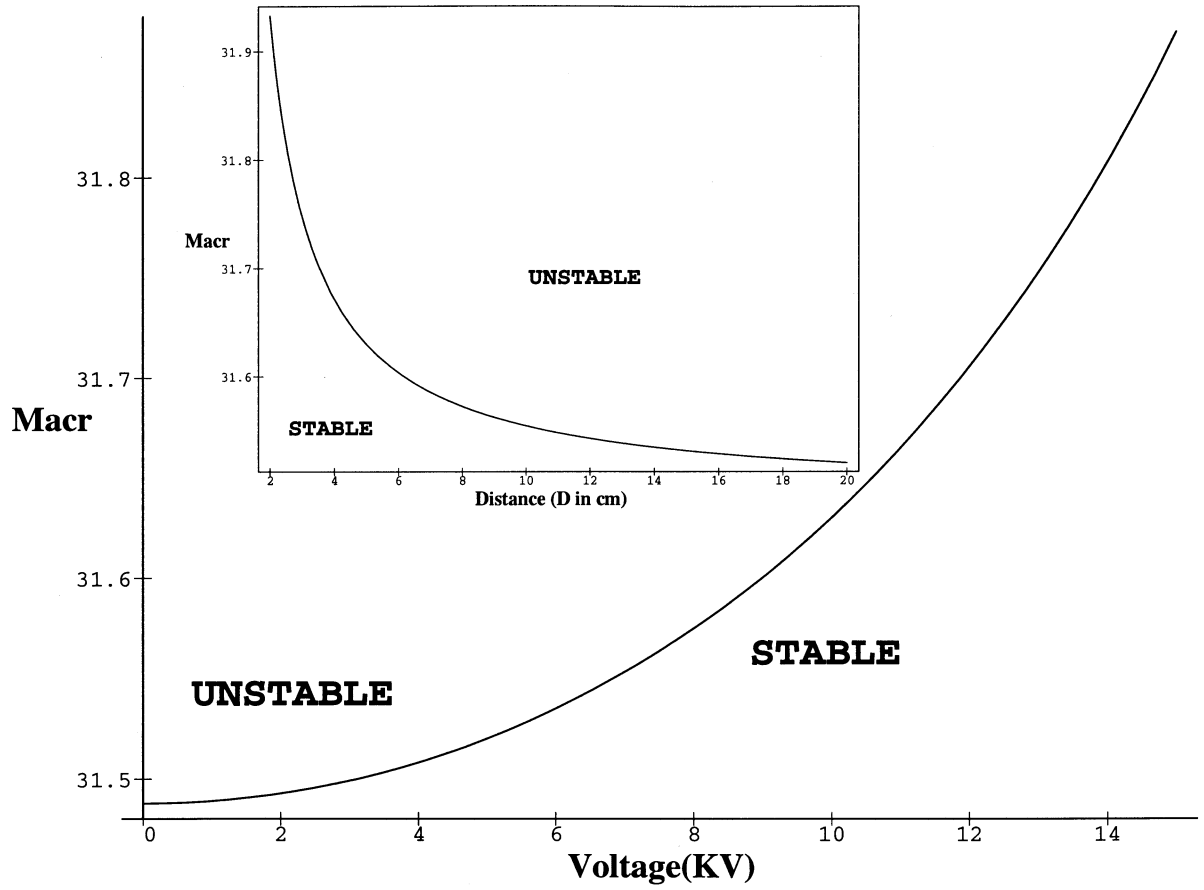

Figure 8. Critical Marangoni number as a function of the applied voltage (kV).

The effect of the spacing (D) is plotted to emphasize the effective influence of the electrical field. $H_i = 0$, $C_r = 10^{-3}$, $N_\mu = 300$, $R_e = 0.01$, $P_r = 30$, $B_r = 0$, $N_\rho = 10^5$.

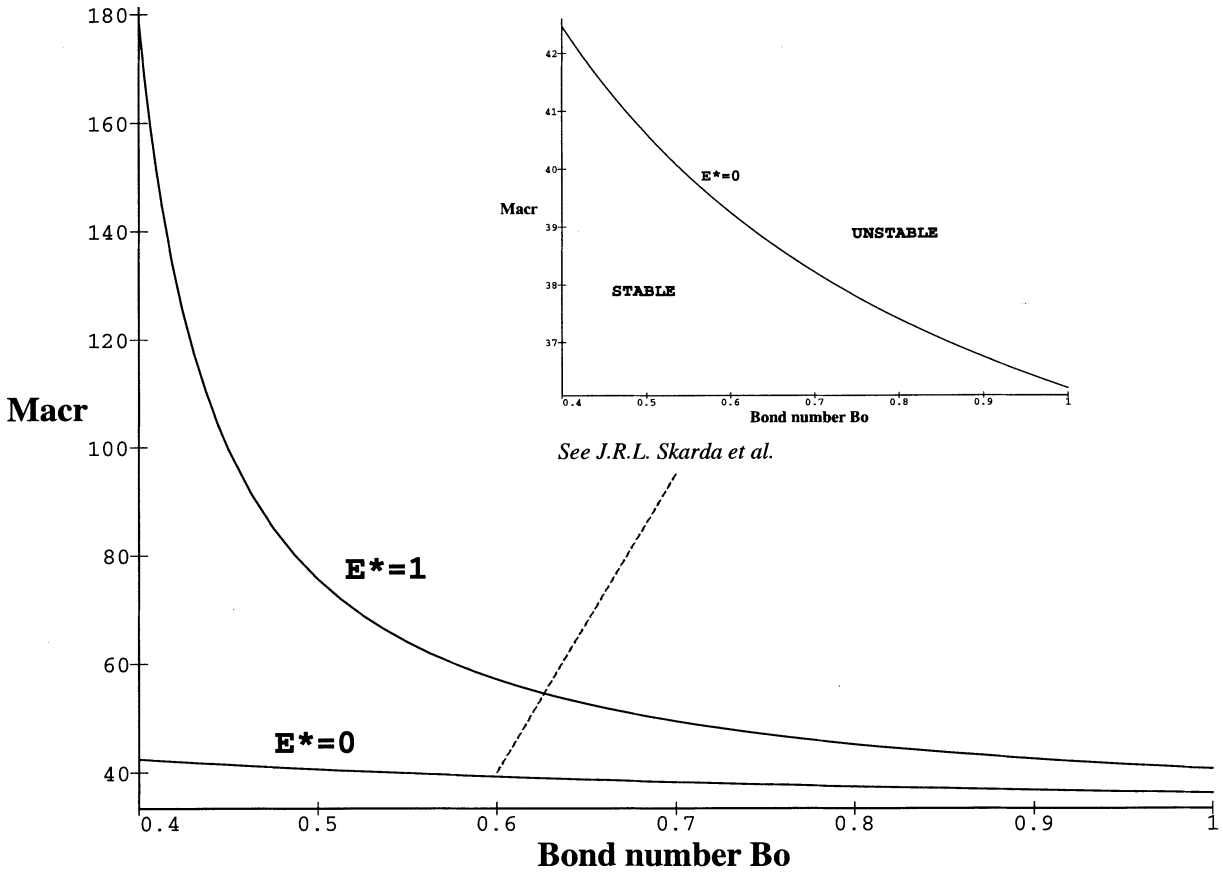

Figure 9. Critical Marangoni number vs. Bond number for different electrical number.

$H_i = 0$, $C_r = 10^{-3}$, $N_\mu = 300$, $R_e = 0.01$, $P_r = 30$, $B_r = 0$, $N_\rho = 10^5$.

is found to increase when decreasing the Bond number. This result is in agreement with the solution found by Skarda and McCaughan (1999). However, this trend is emphasized in the presence of the electrical field (Figure 9). The case for $E^* = 0$ (without electrical field) agrees with the trend described by Skarda and McCaughan (1999).

It was emphasised in previous works (Katto, 1994) that the boiling crisis is found to behave differently under low pressure. In our previous work (Sefiane et al., 1998), we proposed different mechanisms for destabilization at the evaporating meniscus and found that one kind of instability is likely to prevail, depending on the conditions. At low pressure the vapor/liquid density ratio is high enough to promote recoil instability; however, at higher pressure, thermocapillary instability would prevail. In the following section we investigate the influence of the electrical field on the thermocapillary instability as the vapor/liquid density ratio is increased, equivalent to a decrease in pressure. We found the stabilizing effect of the electrical field to be enhanced at lower pressure (Figure 7).

From Figure 10 it can be concluded that the electrical field would have a more pronounced enhancing effect at lower density ratios. At higher density ratios, which may correspond to lower pressure, the effect of the electrical fields is less remarkable.

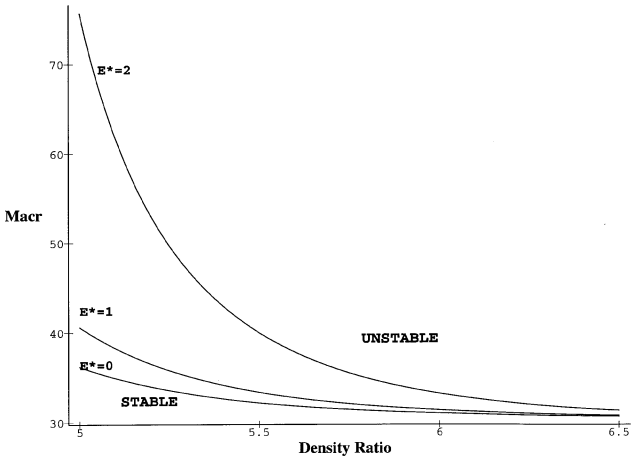

Figure 10. Critical Marangoni number vs. density ratio for different electrical number.

$H_i = 0$, $C_r = 10^{-3}$, $N_\mu = 300$, $R_e = 0.01$, $P_r = 30$, $B_r = 0$, $B_o = 1$.

Perspectives

Our approach provides a physical basis for further studies of the critical heat-flux phenomenon. The enhancement tech-

niques widely used to improve boiling heat transfer could find in this approach improved ways in which the influence of these enhancement methods can be modeled, starting from the local conditions at the triple lines. Other instabilities may prevail, especially at low pressure, where the density ratio is high enough to give rise to recoil instability. The driving force of such instability is the density ratio of the liquid-to-vapor phase.

The thermocapillary instability investigated in this article is found to work over tenths of seconds (Pratt et al., 1998). The recoil instability, as introduced in the analysis of Palmer (1976) and later by Prosperetti and Plesset (1984), is found to occur over hundredths of seconds. The fact that these instabilities operate at a very short time scales makes observations very difficult in the case of boiling heat transfer. We propose that new experiments should be designed for the investigation of boiling heat transfer, focusing on this region.

In the proposed mechanism the wetting parameters are of primary importance. Previous works have demonstrated the influence of these parameters. A more complete understanding of the role of the contact angles of liquids in boiling crisis mechanism is still under investigation. We propose new experiments to elucidate the effective role of wetting in the boiling transition.

Conclusion

In this work, we propose a mechanism for the occurrence of boiling critical heat flux, based on thermocapillary instability. This is likely to contribute at some stage to the destabilization of the steady evaporating meniscus. This approach opens up new avenues in the modeling of the enhancement techniques employed to improve boiling heat transfer. In order to apply this new approach, the modeling of the electrohydrodynamically enhanced boiling has been investigated.

The stability of an evaporating meniscus, under the action of an electrical field has been investigated to find out the parameters influencing the onset of thermocapillary instability.

It has been demonstrated that the application of the electrical field tends to delay thermocapillary instability. The stabilizing effect of the electrical field in the evaporation of a meniscus is a key to the understanding of the enhancement role of electrical-field application.

Notation

$\tilde{A}$ = dimensionless quantity (scaled) A
A' = perturbed quantity A
A^* = Quantity A corresponding to steady state
B' = interfacial displacement
X_i = abscissa of the triple line (Figure 2)
E = electrical field
H_{fg} = latent heat of vaporization
P = pressure
u = velocity vector
W = y-component of the hydrodynamic velocity
J = evaporation rate
$\nabla_{//}$ = Surface derivation operator, $\nabla(\partial^2/\partial x^2) + (\partial^2/\partial z^2)$
k = wave number in x-direction
t = the unit tangent vector
n = the unit normal vector
T = temperature
$\tilde{T}_L, \tilde{T}_v$ = stress tensors in liquid, vapor
k_L, k_v = heat conductivity in liquid, vapor
E^0 = electric field in steady state
v^i = velocity of the interface

Greek letters

δ = Thermal boundary-layer thickness
ϵ = electrical permitivities
β = temperature gradient in thermal layer, $\partial T/\delta$
δ = depth of the thermal boundary layer
θ = angle covered by the liquid meniscus
ρ = density
κ = Thermal diffusivity
ν = Cinematic viscosity
μ = dynamic viscosity
σ = surface tension

Subscripts and superscripts

L = liquid
v = vapor
$*$ = unperturbed state
i = interface
cr = critical

Dimensionless numbers

$$\text{Hickman number} = H_i = \left(\frac{\partial j}{\partial T}\right)\frac{j^*\beta\delta^2\mu_v}{\rho_L\kappa_L\sigma^*}(\rho_v^{-1} - \rho_L^{-1})$$

$$\text{Electrical number} = E^* = \frac{\epsilon_v E^0\delta}{\sigma^*}$$

$$\text{Marangoni number} = M_a = -\frac{\partial\sigma}{\partial T}\frac{\beta\delta^2}{\mu_L\kappa_L}$$

$$\text{Reynolds number} = R_e = \frac{j^*\delta}{\mu_L}$$

$$\text{Crispation number} = C_r = \frac{\mu_L\kappa_L}{\sigma^*\delta}$$

$$\text{Prandtl number} = P_r = \frac{\nu_L}{k_L}$$

$$\text{Bond number} = B_o = \frac{\delta^2 g(\rho_L - \rho_V)}{\sigma^*}$$

$$\text{Brinskman number} = B_r = \frac{W_L^*\nu_L^2}{\beta k_L\delta^2}$$

$$\text{Density ratio} = N_\rho = \frac{\rho_L}{\rho_v}$$

$$\text{Viscosity ratio} = N_\mu = \frac{\mu_L}{\mu_v}$$

Literature Cited

Allen, P. H. G., and T. G. Karayiannis, "Electrohydrodynamic Enhancement of Heat Transfer and Fluid Flow," *Heat Recovery Sys. CHP*, **15**, 389 (1995).

Asch, V., "Electrokinetic Phenomena in Boiling Freon-113," *J. Appl. Phys.*, **37**, 2654 (1966).

Berghmans, J., "Electrostatic Fields and the Maximum Heat Flux," *Int. J. Heat Mass Transfer*, **21**, 791 (1978).

Bergles, A.E., "Heat Transfer Enhancement—The Encouragement and Accommodation of High Heat Fluxes," *Trans. ASME, J. Heat Transfer*, **1**(8) (1997).

Bologa, M. K., S. M. Klimov, and A. N. Maiboroba, "Heat Exchange and Boiling Crisis in Slot Channels Under the Action of an Electric Field," *J. Eng. Phys*, **54**, 59 (1988).

Chubb, L. W., "Improvement Relating to Methods and Apparatus for Heating Liquids," UK Patent No. 100796 (1916).

Choi, H. Y., "Electrohydrodynamic Boiling Heat Transfer," PhD Thesis Dept. of Mechanical Engineering, MIT, Cambridge, MA (1962).

Collier, J. G., *Convective Boiling and Condensation*, Chaps. 8 and 9, McGraw-Hill, New York, p. 236 (1972).
Di Marco, P. and W. Grassi, "Pool Boiling with an Imposed Electric Field: Theoretical Aspects and Experimental Results," *Eur. Two-Phase Flow Group Meeting*, Hertogenbosch, The Netherlands (1995).
Ervin, J. S., H. Merte, Jr., R. B. Keller, and K. Kirk, "Transient Pool Boiling in Microgravity," *Int. J. Heat Mass Transfer*, **3**, 659 (1992).
Haramura, Y., and Y. Katto, "A New Hydrodynamic and Surface Effects on the Peak Heat Flux Applicable Widely to Both Pool and Forced Convection Boiling on Submerged Bodies in Saturated Liquids," *Int. J. Heat Transfer*, 389 (1983).
Hickman, K., "Surface Behavior in the Pot Still," *Ind. Eng. Chem.*, 44 (1952).
Johnson, R. L., "Effect of an Electric Field on Boiling Heat Transfer," *AIAA J.*, **6**, 1456 (1968).
Katto Y., "Critical Heat Flux," *Int. J. Multiphase Flow*, 53 (1994).
Lee, H.S., and H. Merte, Jr., "Origin of the Dynamic Growth of Vapor Bubbles Related to Vapor Explosions," *J. of Heat Transfer*, 174 (1998)
Markels, M. and R. L. Durfee, "The Effect of Applied Voltage on Boiling Heat Transfer," *AIChE J.*, **10**, 106 (1964)
Markels, M., and R. L. Durfee, "Studies of Boiling Heat Transfer with Electric Fields Part I. Effect of Applied AC Voltage on Boiling Heat Transfer to Water in Forced Convection," *AIChE J.*, **11**, 716 (1965).
Palmer, H. J., "The Hydrodynamic Stability of Rapidly Evaporating Liquids at Reduced Pressure," *J. Fluid Mech.*, 487 (1976).
Pratt, D. M., J. R. Brown, and K. P. Hallinan, 'Thermocapillary Effects on the Stability of a Heated, Curved Meniscus," *J. Heat Transfer*, 220 (1998).
Prosperetti, A., and M. S. Plesset, "The Stability of an Evaporating Liquid Surface," *Phys. Fluids*, **7**, 1590 (1984).
Reay, D. A., "Heat Transfer Enhancement—A Review of Techniques and Their Possible Impact on Energy Efficiency in the UK," *Heat Recovery Syst. CHP* **11**, 1 (1991).
Sadasivan, P., C. Unal, and R. Nelson, "Perspective: Issues in CHF Modelling—The Need for New Experiments—," *J. Heat Transfer*, 558 (1995).
Sefiane, K., D. Benielli, and A. Steinchen, "A New Mechanism For Boiling Crisis Recoil Instability and Contact Angle Influence," *Colloids Surf.*, **142**, 361 (1998).
Skarda, J. R. L, F. E. McCaughan, "Exact Solution to Stationary Onset of Convection Due to Surface Tension Variation in a Multicomponent Fluid Layer with Interfacial Deformation," *Int. J. Heat Mass Transfer*, **13**, 42, 2387 (1999).
Straub, J., "Boiling Under Microgravity Conditions," *Proc. Eur. Symp.*, Ajaccio, Corsica, p. 269 (1991).
Takahashi, K., A. Yabe, and H. Maki, "Ectrohydrodynamical (EHD) Research of Saturated Boiling Heat Transfer—Critical Heat Flux on Small Scale Surface and Measurement by Capacitance Probe," *Heat Transfer*, **5**, 153 (1994).
Verplaetsen, F., and J. A. Berghams, "The Influence of an Electric Field on the Heat Transfer Rate during Film Boiling of Stagnant Fluids," *Eurotherm Sem. No. 48*, Germany, p. 327 (1996).
Wayner, P. C., "Thermal Effects in the Spreading of a Liquid Film Due to a Change in the Apparent Finite Contact Angle," *J. of Heat Transfer*, **4**, 938 (1994).
Winer, M., "An Experimental Study of the Influence of a Non-Uniform Electric Field on Heat Transfer in a Dielectric Fluid," *TRW Systems Rep.*, Report No. EMl7-14 TRW Corp., Redondo Beach, CA (1967).
Yabe, A. , Y. Mori, and K. Hijikata, "Active Heat Transfer Enhancement by Utilising Electric Fields," *Annual Review of Heat Transfer*, C. L.Tien, ed, Vol. 7, p. 193 (1996).
Zhorzholiani, A. G., and I. G. Shekriladze, "Study of the Effect of an Electrostatic Field on Heat Transfer with Boiling Dielectric Fluids," *Heat Transfer-Sov. Res.*, **4**, 81 (1972).
Zuber, N., "On the Stability of Boiling Heat Transfer, *Trans. Amer. Soc. Mech. Engi.*, 711 (1958).

Manuscript received June 6, 2000, and revision received May 10, 2001.